Inorganic Chemistry

Article

pubs.acs.org/IC

Carbon-Induced Ferromagnetism in the Antiferromagnetic Metallic Host Material Mn_3ZnN

Ying Sun,*[,†] Yanfeng Guo,[‡] Yoshihiro Tsujimoto,[†] Jiajia Yang,[§] Bin Shen,[§] Wei Yi,[†] Yoshitaka Matsushita,[∥] Cong Wang,[⊥] Xia Wang,[‡] Jun Li,[‡] Clastin I. Sathish,[‡,⊗] and Kazunari Yamaura*[,‡,⊗]

[†]International Center for Materials Nanoarchitectonics (WPI-MANA) and [‡]Superconducting Properties Unit, National Institute for Materials Science, 1-1 Namiki, Tsukuba, Ibaraki 305-0044, Japan

[§]National Research Center for Geoanalysis, 26 Baiwanzhuang, Beijing 100037, China

[∥]Materials Analysis Station, National Institute for Materials Science, 1-2-1 Sengen, Tsukuba, Ibaraki 305-0047, Japan

[⊥]Center for Condensed Matter and Materials Physics, Department of Physics, Beihang University, Beijing 100191, China

[⊗]Graduate School of Chemical Sciences and Engineering, Hokkaido University, Sapporo, Hokkaido 060-0810, Japan

Supporting Information

ABSTRACT: Carbon-for-nitrogen substitution (51 at% at most) was achieved in the antiferromagnetic metallic host material Mn_3ZnN. The various carbon-doped compounds were studied using synchrotron X-ray diffraction, and their electrical resistivities, specific heats, and degrees of magnetization were measured for temperatures of 2−400 K. The sharp antiferromagnetic-to-paramagnetic transition of the host material at 185 K broadened markedly as the carbon content was increased, and a significant ferromagnetic character was found to coexist with the antiferromagnetism when the carbon concentration exceeded 27 at%. This critical magnetic behavior is likely in part due to the increase in the density of states at the Fermi level and the increase in the distance between neighboring Mn atoms. The exact mechanism responsible for the induction of the complicated magnetic state could not be determined. However, the results demonstrate clearly that the chemical tuning of the *X* site in antiperovskite Mn_3AX materials is as useful as that of the *A* and Mn sites and can be used to develop the properties of these materials for practical applications.

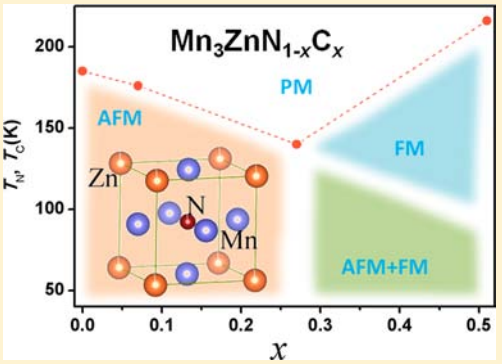

INTRODUCTION

The antiperovskite compounds Mn_3AX (*A* = Cu, Zn, Ga, Cu, and Sn; *X* = C and N) exhibit a great variety of electromagnetic[1−3] and lattice[4−6] properties. These properties may be mutually correlated. Mn-based materials such as Mn_3GaC (which exhibits giant magnetoresistance),[7] Mn_3CuN (magnetostriction),[8] $Mn_3Cu(Ge)N$, and $Mn_3Zn(Ge)N$ (negative thermal expansion or NTE),[9,10] and Mn_3ZnN (phase separation)[11] have already attracted wide interest. However, more studies on these interesting properties of Mn-based materials are needed before they can be exploited for practical applications.[12,13]

To date, much progress has been made related to the design of Mn-based materials by the chemical doping (or substitution) of various species at the *A* site. For instance, a large NTE coefficient (-25×10^{-6} K^{-1}) was achieved in the case of Mn_3CuN by doping Ge at the Cu site.[14] The magnetotransport properties of Mn_3AX compounds were noticeably improved by substitutions in the forms of $Mn_{3+x}Sn_{1-x}C$ and $Mn_3Zn_ySn_{1-y}C$.[15] An extremely low temperature coefficient of resistivity (as low as 10^{-6} K^{-1}) over a wide temperature range was achieved by a partial Ag-for-Cu substitution in Mn_3CuN.[16] Drastic changes in magnetic properties, electronic transport, and lattice contraction could be obtained in $Mn_3Zn_{1-x}Ge_xN$ and $Mn_3Ga_{1-x}Si_xN$.[10,17,18] Meantime, doping at the Mn site was also found to be effective in the development of properties. Magnetic studies of $Mn_{3-x}M_xGaC$ (*M* = Cr or Fe) have shown that the first-order lattice transition resulted in the compounds only after 2% Fe- (or Cr-) substitution of Mn.[19] The partial substitution of Mn with Fe altered the magnetic properties, the extent of the magnetocaloric effect, and the positive magnetoresistance of the antiperovskite $SnCMn_{3-x}Fe_x$ materials (x = 0.05−0.20) drastically as well.[20]

In contrast to the studies investigating doping at the *A* or Mn sites, there have been fewer studies that have looked at the doping of the *X* site. As reported previously, *X* is directly related to the density of states (DOS) at the Fermi level (E_F).[12] Hence, doping at the *X* site should drastically change the electromagnetic properties of the Mn_3AX compounds. Indeed, the Mn-based antiperovskite nitrides and carbides exhibit different physical characteristics, even though they differ in terms of a

Received: September 4, 2012
Published: January 7, 2013

   dx.doi.org/10.1021/ic3019265 | *Inorg. Chem.* 2013, 52, 800−806

single 2p electron. For instance, giant magnetoresistance and the magnetocaloric effect were observed only in the carbides,[7,21,22] while the broadening of the NTE window and the near-zero temperature coefficient of resistivity were noticed only in the nitrides.[10,14,23,24]

In this study, we have tried to increasingly replace the nitrogen in the host material Mn_3ZnN with carbon to test the effect of *X*-site substitution on the materials' properties. As far as we know, this is the first study on the C/N solid solution of Mn_3ZnN. We were able to increasingly substitute carbon for nitrogen (up to 51 at% of carbon, yielding $Mn_3ZnN_{1-x}C_x$, with $0 \leq x \leq 0.51$) successfully. We report the changes in the electromagnetic, thermodynamic, and lattice properties observed in the present study.

EXPERIMENTAL SECTION

Polycrystalline $Mn_3ZnN_{1-x}C_x$ with starting compositions of $x = 0$, 0.1, 0.3, and 0.5 was prepared using fine powders of Mn_2N, Mn (99.99%, Wako Pure Chemical Industries), Zn (99.9%, Rare Metallic Co.), and C (99.9%, Tokai Carbon Co.) via a solid-state reaction. The precursor compound Mn_2N was prepared from the Mn powder by heating it in nitrogen at 800 °C for 60 h. The powders were mixed well in the appropriate compositions, and the resulting mixtures were then pressed into pellets. These pellets were sealed in an evacuated quartz tube and heated at 800 °C for 3 d in a box furnace.

The crystal structure of each compound was analyzed by synchrotron X-ray diffraction (SXRD) using a large Debye–Scherrer camera at the BL15XU beamline of the SPring-8 facility in Hyogo, Japan. The SXRD data were collected for 2θ ranging from 2° to 60° at an interval of 0.03°. The incident beam was monochromatized at λ = 0.65297 Å. Fine powders of each of the compounds, which were ground, were placed in a Lindemann glass capillary (having an inner diameter of 0.2 mm), which was rotated during the measurements.

To evaluate the true carbon content of the synthesized products, we attempted to analyze the products using an electron probe microanalyzer (EPMA) (JXA-8500F, JEOL). However, it was difficult to do so owing to interference from the carbon in the environment. Alternatively, we have tried use a thermogravimetric analyzer under various conditions for the same purpose. However, our attempts have been unsuccessful thus far. In contrast, an elemental analyzer (vario MACRO cube, ELEMENTAR) was successful to measure the true carbon content. Each sample was weighed in a tin vessel and loaded into a carousel and transferred to a combustion tube in a fully automated process, followed by flushing in helium. The catalytic combustion was carried out at a permanent temperature of 1150 °C or below. The formed gas of CO_2 indicated that the true carbon content was 0, 0.07, 0.27, and 0.51 per the formula unit for the samples with the starting compositions $x = 0$, 0.1, 0.3, and 0.5, respectively. As has also been mentioned later, analysis of the SXRD patterns indicated the excellent quality of the products over the entire composition range. In addition, a systematic change in the lattice parameter was also clearly observed as function of the carbon concentration. Hence, the carbon substitution till up to 51 at% did take place during the heat treatment.

The degree of direct current (dc) magnetization of each compound was measured over the temperatures of 2–400 K using a magnetic property measurement system (MPMS) (Quantum Design, Inc.). A portion of the sintered pellet was ground, and the loosely gathered powder placed in a sample holder. The powder was then cooled to the lowest temperature of the temperature range (2 K) in the absence of a magnetic field. Then, a magnetic field with a strength of 0.1 kOe or 5 kOe was applied to the sample. The sample was slowly warmed to 400 K (zero-field cooling or ZFC) and then cooled in the field (field cooling or FC) to 2 K. A magnetic hysteresis loop between −50 kOe and 50 kOe was recorded at a fixed temperature using the same apparatus.

A physical properties measurement system (PPMS) (Quantum Design, Inc.) was used to measure the electrical resistivities (ρ) of the polycrystalline pellets at temperatures of 2–400 K. The pellets were first cooled and then heated and their electrical resistivities measured using the four-point-probe technique with an alternating current (ac) of 10 mA at a frequency of 30 Hz. The electrical contacts were made on the surface of each pellet using silver paste and Pt wires. The surface was carefully polished to remove possible contaminants prior to the wiring. Specific heat (C_p) measurements were performed using the same apparatus at temperatures of 2–400 K upon being cooled by a time-relaxation method. To accurately measure the sample C_p, the C_p of the adhesive grease was also measured prior to the sample measurement. This value was then subtracted from the total C_p.

RESULTS AND DISCUSSION

The crystal structures of the $Mn_3ZnN_{1-x}C_x$ compounds were analyzed by SXRD using the RIETAN software package.[25] In Figure 1, we can see the SXRD patterns for the $Mn_3ZnN_{1-x}C_x$

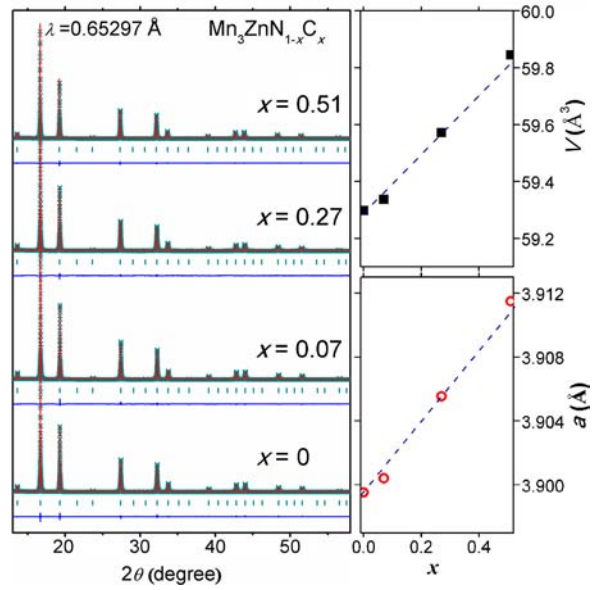

Figure 1. (Left) Rietveld analysis of the SXRD patterns for $Mn_3ZnN_{1-x}C_x$ observed at room temperature. The cross marks and solid lines show the observed and calculated patterns, respectively. The difference between them is shown at the bottom of each panel. The positions of the Bragg reflections are marked by ticks. (Right) Variations in the cubic lattice parameters as a function of *x*. The error bars are smaller than the data markers.

compounds observed at ambient temperature and pressure. An initial analysis of all the patterns was carried out by assuming a $Pm\bar{3}m$ unit cell with N(C), Zn, and Mn atoms at the 1*a* site (0,0,0), 1*b* site (1/2, 1/2, 1/2), and 3*d* site (1/2, 0, 0), respectively. As a result, all the diffraction peaks could be characterized as well as those for other antiperovskite materials.[11] To test a possible anomaly such as a tetragonal distortion, other structural models, including the *P*4/*mmm* model,[12] were tested in the same manner. However, there were no further improvements in the fitting quality, indicating that the $Pm\bar{3}m$ model is the best-fit structure. It is worth noting that peaks related to impurities were not noticeable in any of the patterns, indicating the excellent quality of the compounds prepared.

The cubic lattice constant was calculated by the analysis of the SXRD patterns and is displayed on the right in Figure 1 along with the cubic unit cell volume as a function of the carbon concentration. The lattice constant increased steadily and showed an increase of up to 0.3% (x = 0.51) with an

dx.doi.org/10.1021/ic3019265 | Inorg. Chem. 2013, 52, 800–806

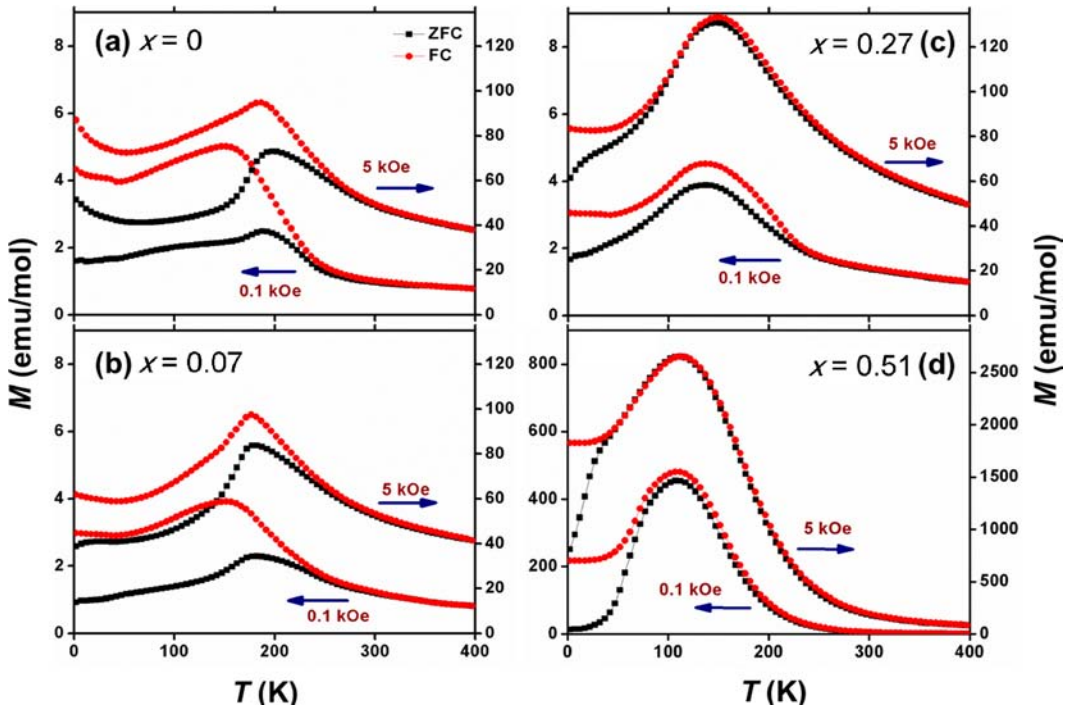

Figure 2. (a–d) Temperature dependence of the magnetization of the $Mn_3ZnN_{1-x}C_x$ compounds in applied magnetic fields of strength of 0.1 kOe and 5 kOe. Note that the panels (a–c) share the common horizontal scale for easy comparison, while the panel (d) uses a scale 2 orders of magnitude larger than used in the other panels.

increase in the carbon content. This result is most likely due to the atomic radius of carbon being greater than that of nitrogen. The plot also indicates that carbon did indeed replace nitrogen in the cubic structure as designed.

The physical properties data of the compounds, shown later, also indicated that the substitution was successful. Note that further synthesis attempts to substitute nitrogen with carbon in concentrations greater than 51 at% using the heat-treatment conditions resulted in the coexistence of two cubic phases, which had different lattice parameters. These two-phase compounds will be investigated in a future study.

Because most of the changes in the electromagnetic properties of the antiperovskite materials seem to be triggered by a magnetic transition,[1−6] we investigated the magnetic properties of the compounds in detail. The host material Mn_3ZnN exhibits an antiferromagnetic (AFM) transition at around 185 K.[10] When x = 0.07, the corresponding magnetic transition appears at 176 K in the ZFC curve and at 160 K in the FC curve in a magnetic field with a strength of 0.1 kOe. The transition temperature was determined by an analysis of the peak positions in the magnetization curves. The transition temperature decreases further, to 140 and 110 K at x = 0.27 and 0.51, respectively. We repeated the measurements in a magnetic field with strength of 5 kOe, and the observed curves are plotted in Figure 2 as well. The 5-kOe-field plots clearly reveal that the transition temperature is almost independent of the strength of the magnetic field, although the thermal hysteresis between the FC and ZFC curves becomes less pronounced. It is possible that the thermal hysteresis observed between the ZFC and FC curves is due to a spontaneous alignment of random magnetic moments of Mn atoms in the domain boundaries as described previously.[26]

To further investigate the magnetic properties of the compounds, the Curie–Weiss law was used to analyze the data. The spin-only expression: $\chi(T) = C/(T - \Theta_W)$, where C is the Curie constant and Θ_W is the Weiss temperature, was applied to the paramagnetic linear region of the H/M-T plot as shown in Figure 3. At x = 0.07, a negative Θ_W of −50 K was

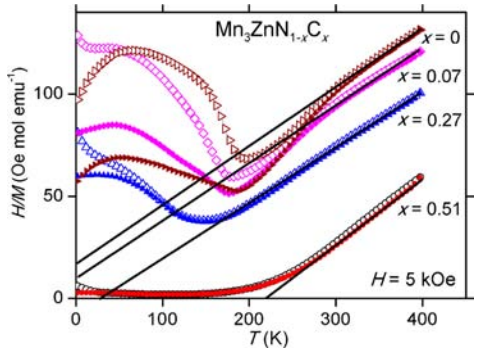

Figure 3. Temperature dependence of the inverse magnetization of the $Mn_3ZnN_{1-x}C_x$ compounds. The solid lines correspond to a linear fit.

obtained, further confirming that the AFM interactions were still dominant in the partially carbon-substituted compounds. However, a positive Θ_W of 25 K was obtained at x = 0.27 and 216 K at x = 0.51, suggesting that the AFM interactions were no longer dominant in the compounds. The sign change of Θ_W suggests that ferromagnetic (FM) interactions develop quickly in the material with an increase in the carbon concentration. The FM interactions were confirmed by the M-H measurements as follows.

The left panel of Figure 4 shows the field-strength dependence of the isothermal magnetization of the $Mn_3ZnN_{1-x}C_x$ compounds at different temperatures. For $x \leq$ 0.27, the M-H curves are fundamentally linear, even well below

dx.doi.org/10.1021/ic3019265 | Inorg. Chem. 2013, 52, 800–806

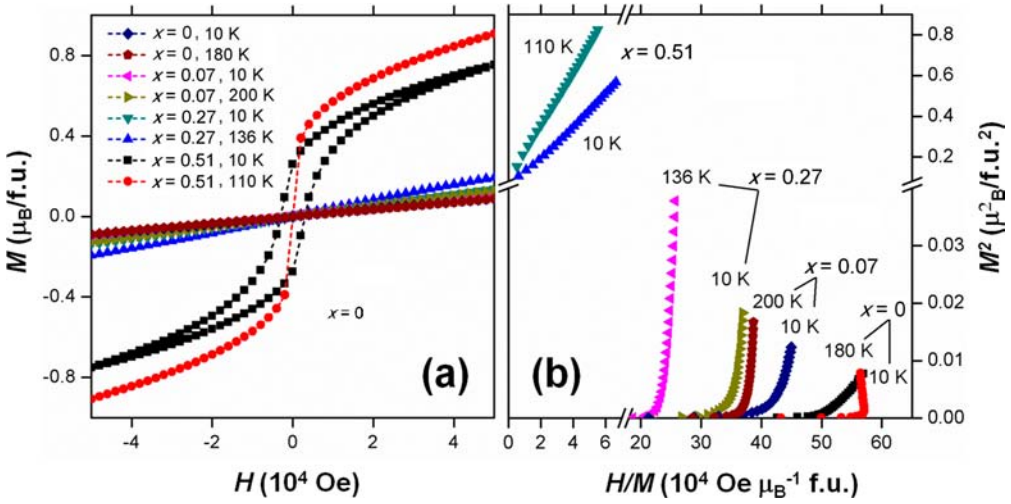

Figure 4. (a) Isothermal magnetization of the compounds of $Mn_3ZnN_{1-x}C_x$ at various temperatures, and (b) Arrott plot of the magnetization data.

the magnetic-transition temperature (determined from the *M-T* measurements), which was indicative of an AFM order. When x is increased to 0.51, the corresponding *M-H* curves exhibit hysteresis clearly, indicating that FM interactions are dominant. The *M-H* curves, however, did not tend toward magnetic saturation, suggesting a possible coexistence of the FM and AFM orders. For further analysis of the degree of magnetization, all data were plotted in an alternative form in an "Arrott plot" (the right panel of Figure 4).[27] When the M^2-H/M curves are linearly extrapolated backward, the *X*-axis intercepts change their sign from positive to negative with an increase in the carbon concentration. The analysis also indicated that as the carbon concentration increases, the magnetic states of the $Mn_3ZnN_{1-x}C_x$ compounds undergo a transition from being AFM-order-dominated to one where the AFM and FM orders coexist. The critical carbon concentration between the two states corresponds to $0.27 \leq x \leq 0.51$.

It is clear that the substitution of nitrogen in Mn_3ZnN with carbon induces ferromagnetism. Generally speaking, itinerant magnetism largely depends on the electronic density of states at E_F. However, for materials in the class Mn_3AX, a critical distance d_c between the Mn atoms has often been stated as being a major parameter in the characterization of the magnetic order because the DOS at E_F varies considerably at d_c.[28] Continually increasing the carbon concentration in the compounds may vary the Mn−Mn distance d_{Mn-Mn} from $<d_c$ to $>d_c$ because the Mn atoms are expected to be ordered ferromagnetically at $d_{Mn-Mn} > d_c$ and antiferromagnetically at $d_{Mn-Mn} < d_c$.[28] In the case of the present $Mn_3ZnN_{1-x}C_x$ materials, the critical composition was found to be near x = 0.27, corresponding to a d_{Mn-Mn} of 2.761 Å. $Mn_3Zn_{1-y}Sn_yC$ compounds, in which the FM order is dominant for $y > 0.4$, were found to behave in a similar manner.[15] The critical distance d_c was then estimated to be approximately 2.78 Å for the $Mn_3Zn_{1-y}Sn_yC$ compounds.[15] However, only empirically determined values of the critical d_c, such as in the case of $Mn_3Zn_{1-y}Sn_yC$ compounds, are available. Therefore, it is hard to discuss the nature of the critical distance in the case of the $Mn_3ZnN_{1-x}C_x$ compounds in greater detail.

Alternatively, the dramatic change in the magnetic properties as a result of the carbon-for-nitrogen substitution may also be accounted for, to a certain degree, by the hole−carrier-doping effect. Formally, each N atom in the lattice donates three 2p electrons to the neighboring Mn atoms, thus decreasing the number of unpaired Mn 3d electrons. In comparison, the C atom has only two 2p electrons. Therefore, the carbon-for-nitrogen substitution should increase the number of unpaired Mn 3d electrons, resulting in an increase in the Mn−Mn magnetic-exchange interactions, which, in turn, facilitates the appearance of the FM order.

The increase in the FM interactions in the $Mn_3ZnN_{1-x}C_x$ compounds may break a magnetic balance between the AFM and FM orders, giving rise to the complex magnetic features. The coexistence of the AFM and FM orders is theoretically possible in certain itinerant-electrons systems, as was proposed by Moriya and Usami.[29,30] They expressed the free energy in terms of uniform (M_0) and staggered (M_Q) magnetizations as follows:

$$F = (1/2\chi_0)M_0^2 + (1/2\chi_Q)M_Q^2 + (1/4)\gamma_u M_0^4 + (1/4)\gamma_s M_Q^4 + (1/2)\gamma_{us} M_0^2 M_Q^2 - HM_0$$

Here, χ_0 and χ_Q are the uniform and the staggered susceptibilities, γ_u, γ_s, and γ_{us} are the coefficients of the terms M_0^4, M_Q^4, and $M_0^2M_Q^2$, respectively, and H is a uniform external magnetic field. It has been suggested that when the coupling between M_0 and M_Q is intense (i.e., $\gamma_{us}^2 > \gamma_u \cdot \gamma_s$), a stable, pure FM or AFM state results. On the other hand, when the coupling is weak ($\gamma_{us}^2 < \gamma_u \cdot \gamma_s$), coexisting FM and AFM states emerge. More importantly, all the temperature-induced and field-induced transitions are of the second order within the theoretical considerations. This seems to accord with the magnetic data for the $Mn_3ZnN_{1-x}C_x$ compounds, which suggest that the transition with an increase in the carbon concentration was more likely a second-order than a first-order one (see the temperatures corresponding to the peaks in the ZFC and FC curves in Figure 2).

To study the magnetic nature of the present materials, the temperature dependence of ρ of sintered $Mn_3ZnN_{1-x}C_x$ compounds was investigated, as shown in Figure 5. For x = 0, an abrupt change at the magnetic transition temperature was observed clearly, and this was in keeping with previously reported results.[10] It should be noted that abrupt change is slightly different from that reported in our previous study.[31] This is most likely because in the earlier study, we used different synthesis methods, which have been described

dx.doi.org/10.1021/ic3019265 | Inorg. Chem. 2013, 52, 800−806

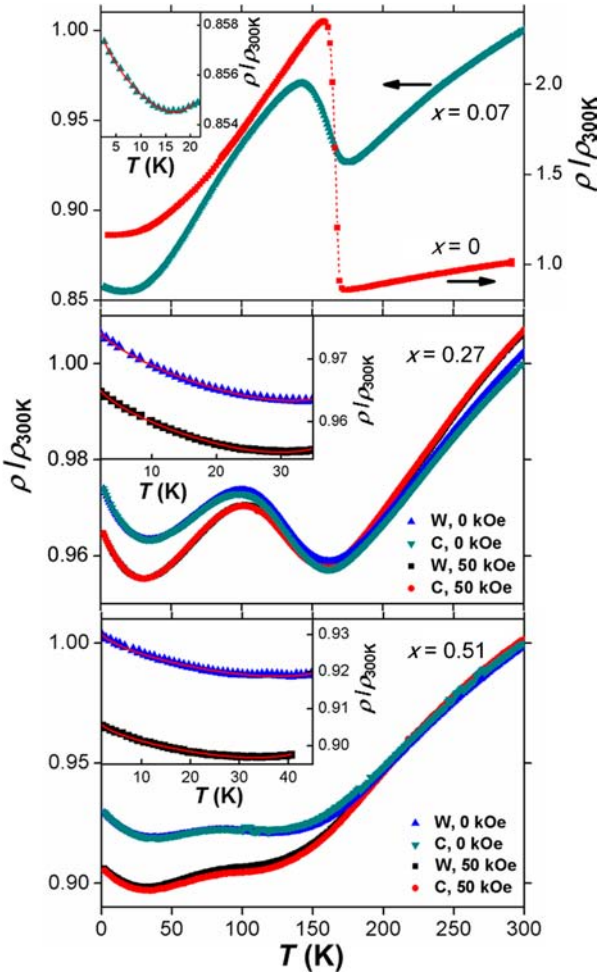

Figure 5. Temperature dependence of the resistivity of sintered $Mn_3ZnN_{1-x}C_x$ compounds in the absence and presence (strength of 50 kOe) of a magnetic field. The inset shows fitting using a function at low temperature; the solid curves correspond to the fitting.

elsewhere.[32] It is also worth noting that the change occurs over a broader range of temperatures with an increase in the carbon concentration: for $x = 0.27$, the broadened temperature range ΔT is ~60 K (101 K ≤ T ≤ 161 K), whereas ΔT is ~30 K (142 K ≤ T ≤ 172 K) for $x = 0.07$ and ~15 K (158 K ≤ T ≤ 173 K) for $x = 0$. In the case of $x = 0.51$, the curves are much flatter, with the change being relatively smaller. The curves for the C_p data exhibit similar broadening as well (shown later).

Another striking feature of the ρ-T curves is the appearance of multiple unusual minima at low temperatures as a result of the carbon substitution. The lowest-temperature minima (ρ_{min}) appear at 17 K, 31 K, and 35 K for $x = 0.07$, 0.27, and 0.51, respectively. Because a normal metal shows only a monotonic change in ρ on cooling, the ρ minima in the case of the $Mn_3ZnN_{1-x}C_x$ compounds must reflect additional scattering factors. It is well-known that the Kondo effect, which arises from the spin scattering of conduction electrons in the vicinity of magnetic atoms, can be responsible for similar ρ minima.[33] As mentioned earlier, the substituted carbon will increase the number of unpaired 3d electrons. If this leads to localized magnetic moments, it would suggest the Kondo effect was responsible for the observed ρ minima. To test whether this was the case, a magnetic field was applied during the ρ measurements. However, as Figure 5 shows, the field had only a minor impact on the ρ minima. If the ρ minima were exclusively due to the Kondo effect, the ρ minima should disappear on the application of the magnetic field as the spin scattering of the conducting electrons would be suppressed markedly. Hence, the fact that there was no change in ρ as a result of the application of the magnetic field suggests that the Kondo mechanism likely plays only a minor role in the occurrence of the ρ minima.

We considered whether other possible models could account for the ρ minima. Electron−electron (e−e) scattering due to Coulomb interactions may explain the additional scattering of charged carriers, as is often the case in a strongly correlated system. Generally, e−e scattering is not affected significantly by a magnetic field.[34,35] Hence, in addition to being partially explained by Kondo scattering, the ρ data may be characterized using the framework of e−e interactions, which would mean that ρ is dependent on $T^{1/2}$ and ln T.[34,35] For quantitative analysis, we use the following equation to fit the low-temperature resistivity data for ρ values smaller than T_{min}:

$$\rho = P_1 - P_2T^{1/2} - P_3 \ln T + P_4T^5$$

where the coefficients P_1, P_2, P_3, and P_4 denote the contributions from the residual resistivity, e−e interactions, Kondo-like spin-dependent scattering, and electron−phonon (e−p) interactions, respectively. As shown in the inset of Figure 5, the curves are fitted well with the equation. The parameters attained from the fitting are summarized in Table 1. These

Table 1. Parameters Used to Fit the Resistivity Data (H = 0 kOe) of the $Mn_3ZnN_{1-x}C_x$ Compounds

x	P_1	P_2	P_3	P_4
0				
0.07	0.86	1.05×10^{-3}	3.91×10^{-4}	3.78×10^{-10}
0.27	0.98	2.64×10^{-3}	4.10×10^{-4}	4.15×10^{-11}
0.51	0.93	2.33×10^{-3}	5.81×10^{-4}	2.01×10^{-11}

results show that P_3 (related to spin scattering) increases with the increase in the carbon concentration, suggesting that the spin scattering tends to intensify as a result of the carbon-for-nitrogen substitution. P_2 appears to increase and then decrease with the increase in the carbon concentration. This suggests that appearance of the FM state may fix the local spin directions and suppress the e−e scattering.

It can be seen that the coefficient related to e−p interactions (P_4) is much smaller than the other coefficients, suggesting that behavior of the ρ minima is mostly determined by the Kondo-like scattering and e−e interactions. Because the Kondo-like scattering plays only a minor role at most, the good agreement between the experimental data and the fitted curves suggests that the unusual ρ minima are mostly due to the e−e interactions. Other possible mechanisms that could cause electron localization may be related to the polycrystalline nature of the present materials, such as grain boundaries scattering. The issue is left for a future study when high-quality single crystals of the $Mn_3ZnN_{1-x}C_x$ compounds become available.

The magnetic transition is accompanied by a peak in the C_p−T curve (Figure 6). The sharp peak in the curve for $x = 0$ corresponds to the AFM transition, as was confirmed by the neutron diffraction spectroscopy of Mn_3ZnN.[10] The peak becomes less sharp and broadens when carbon is substituted for nitrogen, and this observation qualitatively accorded with the

dx.doi.org/10.1021/ic3019265 | Inorg. Chem. 2013, 52, 800−806

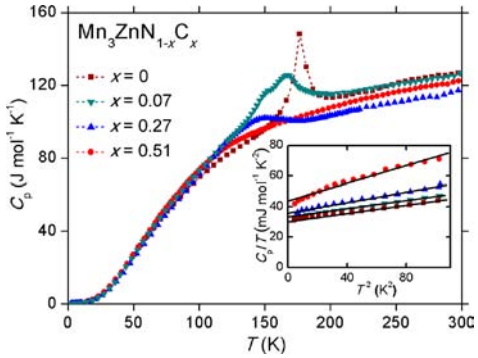

Figure 6. Temperature dependence of the specific heat of the $Mn_3ZnN_{1-x}C_x$ compounds. The inset shows the linear fitting of the C_p data at low temperatures.

broadening noticed in the electrical resistivity curves. In the case of $x = 0.51$, the endothermic peak almost disappears. This may reflect the weakening of the AFM state as a result of the carbon substitution.

According to the Labbé–Jardin tight-binding model, a magnetic transition is correlated to the parameter $|E_F - E_s|$, and in the case of Mn_3AX compounds, E_F lies close to the infinite singularities energy E_s in the electronic DOS.[36] If the doped carbon induces a slight shift in the E_F level, it would result in a change in the parameter $|E_F - E_s|$. This may alternatively account for the broadening of the C_p peaks.[36] Besides, the broadening of the C_p peaks in the case of carbon-doped compounds is phenomenologically similar to what was found for Ge-doped Mn_3CuN; the broadening in the case of the latter was associated with a local T_4 structure.[37] The changes in the local structure became much more significant as the level of Ge doping was increased.[37] That a change in the local structure occurred in the case of the $Mn_3Cu_{1-x}Ge_xN$ compounds was confirmed experimentally by a pair-distribution function analysis of the neutron diffraction data. The local T_4 structure was found to have been caused by an inhomogeneous distribution of Mn–Ge bonds in the corner-shared Mn_6X octahedra.[37] The broadening noticed in the case of $Mn_3ZnN_{1-x}C_x$ is possibly caused by a similar mechanism related to a change in the local structure. Further studies on $Mn_3ZnN_{1-x}C_x$ compounds using neutron diffraction analysis will help reveal a clearer picture as to how the carbon substitution results in the broadening of the C_p peaks.

The C_p data for temperatures below 10 K was further analyzed using the approximate Debye model: $C_p(T)/T \sim \gamma + 2.4\pi^4 n N_0 k_B (1/\Theta_D{}^3) T^2$, where n denotes the number of atoms per the unit cell (5 in this case), k_B is the Boltzmann constant, and N_0 is the Avogadro constant. The Sommerfeld coefficient γ and the Debye temperature Θ_D were determined by fitting the linear parts of the C_p/T vs T^2 curves (see the inset of Figure 6). The obtained values were $\gamma = 31.3$, 32.7, 36.8, and 43.3 mJ mol^{-1} K^{-2}, and $\Theta_D = 428$, 408, 378, and 320 K for $x = 0$, 0.07, 0.27, and 0.51, respectively. The values of γ are relatively larger than that for a pure 3d metal, indicating a relatively higher DOS at E_F.[38]

The value of γ increased with an increase in the carbon concentration. If we presume that a free electron gas model effectively represents the present electronic system, the number of DOS at E_F $[N(E_F)]$ can be estimated from the γ value via the following equation:

$$\gamma = (1/3)\pi^2 \kappa_B{}^2 N(E_F)$$

Thus, a higher γ value implies an increase in $N(E_F)$. The electronic structure of the Mn_3AN compounds shows a DOS peak always below E_F regardless of the choice of element A.[36] With an increase in the lattice parameter, the peak may shift from the lower energy level toward E_F, while the entire DOS structure changes little. Hence, $N(E_F)$ increases.[20] In the Stoner model, the criterion for the occurrence of the long-range FM order is $N(E_F)I > 1$, where I represents the exchange integral that reflects the exchange splitting of the energy bands.[39] In this scenario, when $N(E_F)$ increases, so does the product $N(E_F)I$. Therefore, the larger value of γ and the increase in the lattice parameter caused by the carbon substitution are both likely responsible for the appearance of the FM order in the carbon-doped materials. Because these are only possible qualitative explanations, further studies, including theoretical considerations, are needed to quantitatively understand the critical magnetic behavior of the $Mn_3ZnN_{1-x}C_x$ materials for values of x close to 0.27. The relationships between the carbon concentration and the physical properties of the $Mn_3ZnN_{1-x}C_x$ compounds are summarized in Figure 7.

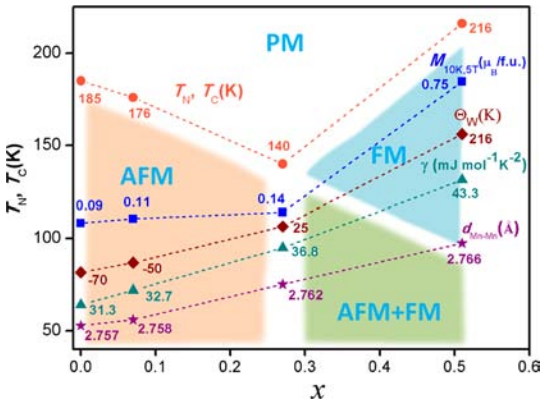

Figure 7. Electromagnetic and lattice parameters of $Mn_3ZnN_{1-x}C_x$ compounds as a function of the carbon concentration x. PM, paramagnetism; AFM, antiferromagnetism; and FM, ferromagnetism.

To summarize, this study reveals that FM characteristics are induced in the purely AFM metallic host material Mn_3ZnN by carbon-for-nitrogen substitution. The host exhibits a sharp AFM transition accompanied by ρ- and C_p-related anomalies. The AFM transition is markedly broadened with an increase in the carbon substitution, indicating a notable change in the AFM state. Unusual minima were observed in the $\rho-T$ curves at low temperatures, which were seemingly caused by e–e scattering. The Sommerfeld coefficient γ derived from the low-temperature C_p data increases continuously with an increase in the carbon content, implying that $N(E_F)$ also increased. The cubic lattice parameter also increases with the increase in the carbon concentration, corresponding to an increment in d_{Mn-Mn}. The increases in the $N(E_F)$ and d_{Mn-Mn} values both stabilize the FM state in the host structure. The critical composition for the $Mn_3ZnN_{1-x}C_x$ compounds between the AFM and FM orders was found to exist at x close to 0.27. The exact mechanism responsible for the appearance of the FM order is not known. However, it was demonstrated clearly that doping at the X site is as effective as doping at the A and Mn sites in improving the properties of the antiperovskite Mn_3AX materials with respect to possible future applications. The phase diagram showing the

dx.doi.org/10.1021/ic3019265 | Inorg. Chem. 2013, 52, 800–806

transitions between Mn_3ZnN and $Mn_3ZnN_{0.49}C_{0.51}$ was determined for the first time, as far as we know. The diagram is quite complicated, even though Mn_3ZnN and $Mn_3ZnN_{0.49}C_{0.51}$ differ in terms of a half 2p electron. Unfortunately, a high-T_c superconductivity, which often emerges near an antiferromagnetic metallic state as a result of doping, is most likely absent.

■ ASSOCIATED CONTENT

Supporting Information

Structural parameters of the $Mn_3ZnN_{1-x}C_x$ compounds. This material is available free of charge via the Internet at http://pubs.acs.org.

■ AUTHOR INFORMATION

Corresponding Author

*E-mail: SUN.Ying@nims.go.jp (Y.S.), YAMAURA.Kazunari@nims.go.jp (K.Y.).

Notes

The authors declare no competing financial interest.

■ ACKNOWLEDGMENTS

The authors would like to thank the staffs of BL15XU, NIMS, and SPring-8 for their help at the beamline. The SXRD measurements were performed under the approval of the NIMS Beamline Station (Proposal No. 2012B4506). This work was supported in part by the World Premier International Research Center Initiative of the Ministry of Education, Culture, Sports, Science, and Technology (MEXT); a Grants-in-Aid for Scientific Research grant (#22246083) from the Japan Society for the Promotion of Science (JSPS); the Funding Program for World-Leading Innovative R&D on Science and Technology (FIRST Program) of the JSPS; and the Advanced Low Carbon Technology Research and Development Program (ALCA) of the Japan Science and Technology Agency (JST).

■ REFERENCES

(1) Kim, W. S.; Chi, E. O.; Kim, J. C.; Choi, H. S.; Hur, N. H. *Solid Sate Commun.* **2001**, *119*, 507.
(2) Ding, L.; Wang, C.; Chu, L. H.; Yan, J.; Na, Y. Y.; Huang, Q. Z.; Chen., X. L. *Appl. Phys. Lett.* **2011**, *99*, 251905.
(3) Wang, B. S.; Tong, P.; Sun, Y. P.; Tang, W.; Li, L. J.; Zhu, X. B.; Yang, Z. R.; Song, W. H. *J. Magn. Magn. Mater.* **2010**, *322*, 163−168.
(4) Naish, V. E. *J. Magn. Magn. Mater.* **1981**, *24*, 299.
(5) Song, X. Y.; Sun, Z. H.; Huang, Q. Z.; Rettenmayr, M.; Liu, X. M.; Seyring, M.; Li, G. N.; Rao, G. H.; Yin, F. X. *Adv. Mater.* **2011**, *23*, 4690.
(6) Takenaka, K.; Takagi, H. *Appl. Phys. Lett.* **2009**, *94*, 131904.
(7) Kamishima, K.; Goto, T.; Nakagawa, H.; Miura, N.; Ohashi, M.; Mori, N.; Sasaki, T.; Kanomata, T. *Phys. Rev. B* **2000**, *63*, 024426.
(8) Asano, K.; Koyama, K.; Takenaka, K. *Appl. Phys. Lett.* **2008**, *92*, 161909.
(9) Iikubo, S.; Kodama, K.; Takenaka, K.; Takagi, H.; Takigawa, M.; Shamoto, S. *Phys. Rev. Lett.* **2008**, *101*, 205901.
(10) Sun, Y.; Wang, C.; Wen, Y. C.; Zhu, K. G.; Zhao, J. T. *Appl. Phys. Lett.* **2007**, *91*, 231913.
(11) Sun, Y.; Wang, C.; Huang, Q. Z.; Guo, Y. F.; Chu, L. H.; Arai, M.; Yamaura, K. *Inorg. Chem.* **2012**, *51*, 7232.
(12) Fruchart, D.; Bertaut, E. F. *J. Phys. Soc. Jpn.* **1978**, *44*, 781.
(13) Kaneko, T.; Kanomata, T.; Shirakawa, K. *J. Phys. Soc. Jpn.* **1987**, *56*, 4047.
(14) Takenaka, K.; Takagi, H. *Appl. Phys. Lett.* **2005**, *87*, 261902.
(15) Li, Y. B.; Li, W. F.; Feng, W. J.; Zhang, Y. Q.; Zhang, Z. D. *Phys. Rev. B* **2005**, *72*, 024411.
(16) Takenaka, K.; Ozawa, A.; Shibayama, T.; Kaneko, N.; Oe, T.; Urano, C. *Appl. Phys. Lett.* **2011**, *98*, 022103.
(17) Kong, X. B.; Sun, Y.; Yang, L. X.; Yu, Y.; Jin, C. Q.; Wang, C.; Yu, R. C. *J. Appl. Phys.* **2009**, *106*, 113905.
(18) Sun, Y.; Wang, C.; Wen, Y. C.; Chu, L. H.; Nie, M.; Liu, F. S. *J. Am. Ceram. Soc.* **2010**, *93*, 650.
(19) Harada, T.; Nishimura, K.; Kanomata, T.; Kaneko, T. *Jpn. J. Appl. Phys.* **1993**, *32*, 280.
(20) Wang, B. S.; Tong, P.; Sun, Y. P.; Tang, W.; Li, L. J.; Zhu, X. B.; Yang, Z. R.; Song, W. H. *J. Magn. Magn. Mater.* **2010**, *322*, 163.
(21) Burriel, R.; Tocado, L.; Palacios, E.; Tohei, T.; Wada, H. *J. Magn. Magn. Mater.* **2005**, *290−291*, 715.
(22) Yu, M. H.; Lewis, L. H.; Moodenbaugh, A. R. *J. Appl. Phys.* **2003**, *93*, 10128.
(23) Chi, E. O.; Kim, W. S.; Hur, N. H. *Solid State Commun.* **2001**, *120*, 307.
(24) Sun, Y.; Wang, C.; Chu, L. H.; Wen, Y. C.; Nie, M.; Liu, F. S. *Scr. Mater.* **2010**, *62*, 686.
(25) Izumi, F.; Ikeda, T. *Mater. Sci. Forum* **2000**, *198*, 321−324.
(26) Galstyan, E.; Lorenz, B.; Martirosyan, K. S.; Yen, F.; Sun, Y. Y.; Gospodinov, M. M.; Chu, C. W. *J. Phys.: Condens. Matter* **2008**, *20*, 325241.
(27) Arrott, A. *Phys. Rev.* **1957**, *108*, 1394.
(28) Gerasimov, E. G.; Gaviko, V. S.; Neverov, V. N.; Korolyov, A. V. *J. Alloys Compd.* **2002**, *343*, 14.
(29) Nishihara, Y.; Yamaguchi, Y. *J. Phys. Soc. Jpn.* **1985**, *54*, 1122.
(30) Moriya, T.; Usami, K. *Solid State Commun.* **1977**, *23*, 935.
(31) Sun, Y. S.; Guo, Y. F.; Wang, X. X.; Tsujimoto, Y.; Matsushita, Y.; Shi, Y. G.; Wang, C.; Belik, A. A.; Yamaura, K. *Appl. Phys. Lett.* **2012**, *100*, 161907.
(32) Wang, C.; Chu, L. H.; Yao, Q. R.; Sun, Y.; Wu, M. M.; Ding, L.; Yan, J.; Na, Y. Y.; Tang, W. H.; Li, G. N.; Huang, Q. Z.; Lynn, J. W. *Phys. Rev. B* **2012**, *85*, 220103.
(33) Kondo, J. *Proc. Jpn. Acad., Ser. B* **2006**, *82*, 328.
(34) Rana, D. S.; Markna, J. H.; Parmar, R. N.; Kuberkar, D. G.; Raychaudhuri, P.; John, J.; Malik, S. K. *Phys. Rev. B* **2005**, *71*, 212404.
(35) Zhang, Z. Q.; Zhang, J. C.; Xu, Y.; Jing, C.; Cao, S. X.; Zhao, Y. G. *Phys. Rev. B* **2006**, *74*, 045108.
(36) Jardin, J. P.; Labbe, J. *J. Solid State Chem.* **1983**, *46*, 275.
(37) Iikubo, S.; Kodama, K.; Takenaka, K.; Takagi, H.; Shamoto, S. *Phys. Rev. B* **2008**, *77*, 020409 (R).
(38) Todd, S. S.; Bonnickson, D. R. *J. Am. Chem. Soc.* **1951**, *73*, 3844.
(39) Tong, P.; Sun, Y. P.; Zhu, X. B.; Song, W. H. *Phys. Rev. B* **2006**, *73*, 245106.